J. Bangladesh Acad. Sci. 50(2); 197–206: June 2026 DOI: https://doi.org/10.3329/jbas.v50i2.90652

Journal of Bangladesh Academy of Sciences

Journal homepage: http://www.bas.org.bd/publications/jbas.html

Research Article

Reaction of $[Os_3(CO)_{10}(NCMe)_2]$ with isatin: Regiospecific μ-(N,O) coordination of the isatinate ligand to the triosmium framework

Md. Mahbub Alam, Shafikul Islam, Nahid Akter, and Shariff E. Kabir*

Department of Chemistry, Jahangirnagar University, Savar, Dhaka 1342, Bangladesh

ARTICLE INFO

Article History

Received: 24 February 2026
Revised: 12 March 2026
Accepted: 15 April 2026

Keywords: Triosmium, Isatinate, Regiospecific μ-(N,O) coordination, X-ray crystal structure, DFT study.

ABSTRACT

Treatment of activated $[Os_3(CO)_{10}(NCMe)_2]$ cluster with isatin (1H-indole-2,3-dione) at room temperature furnished a new hydrido-bridged triosmium isatinate complex, $[Os_3(CO)_{10}(\mu\text{-}H)(\mu\text{-}\kappa^1(N)\kappa^1(O)\text{-}C_6H_4(CO)_2N)]$ (**1**) in a moderate yield. The compound is formed through the oxidative N–H bond activation, accompanied by regiospecific μ-(N,O) coordination to the Os_3 framework. Characterization of **1** was done by elemental analysis, infra red, spectroscopy, ^{1}H NMR spectroscopy, and X-ray diffraction analysis. The bonding in **1** has been investigated based on the density functional theory (DFT) method. The DFT-optimized geometry is similar to its solid state structure and the simulated structure parameters are in good agreement with the measured values.

Introduction

Triosmium dodecacarbonyl is a remarkable avenue for the development of clusters resembling catalysis, advanced materials, and fundamental reactivity (Stiefel and Matsumoto, 1996; Hoff, 1992; Darensbourg et al., 1989; Henderson et al., 1987; Lang et al., 1994). However, owing to its low reactivity, this cluster is often converted to its labile intermediate, $[Os_3(CO)_{10}(NCMe)_2]$ (Ju et. al., 1998), prior to the reaction with the desired ligand. Incorporation of heterocyclic ligands (notably sulfur and nitrogen donors) often stabilizes cluster cores under forcing conditions and unlocks new reaction pathways through edge-bridging or face-capping motifs (Darensbourg et al., 1989; Henderson et al., 1987; Lang et al., 1994; Ju et. al., 1998; Russell et al., 2003; Monira et al., 2015). Among heterocycles capable of displaying adaptable coordination behavior, saccharin and thiosaccharin are instructive benchmarks because they can bind metals in mono-, bi-, and bridging modes, frequently through nitrogen and chalcogen/oxygen donors (Ju et. al., 1998; Russell et al., 2003; Monira et al., 2015). For example, the reaction of the labile triosmium precursor, $[Os_3(CO)_{12-n}(NCMe)_n]$ (n = 1–2), undergoes ligand exchange by saccharin moiety at 80 °C (Scheme 1) with concurrent hydride formation by the N–H bond activation (Monira et al., 2015). The bidentate μ-(N,O) saccharinate binding across an Os–Os vector has been reported to persist even after successive carbonyl substitutions by phosphines (Ju et. al., 1998; Russell et al., 2003; Monira et al., 2015).

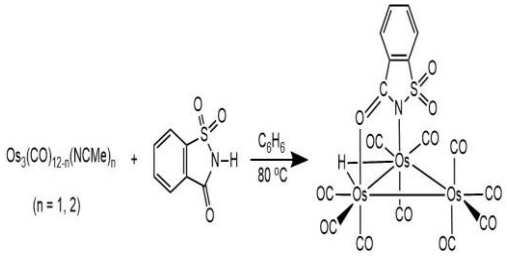

Scheme 1. Synthesis of $[Os_3(CO)_{10}(\mu\text{-}H)(\mu\text{-}sac)]$.

Isatin (1H-indole-2,3-dione) is historically obtained by oxidative transformation of indigo and has since become a privileged synthon for the generation of condensed frameworks and functionalized ligands

*Corresponding author:<skabir_ju@yahoo.com>

(Silva et al., 2001). Isatin and its derivatives have been widely documented to exhibit anticancer, cytotoxic, antibacterial, antifungal, antiviral, anticonvulsant, anti-inflammatory, and neuroactive profiles, supporting its characterization as a privileged pharmacophore (Vine et al., 2009; Medvedev et al., 2007). Mechanistic perspectives also emphasize that isatin can modulate cellular pathways and bind diverse biological targets, while derivatization tunes potency and selectivity (Medvedev et al., 2007; Chowdhary et al., 2022). Beyond the organic scaffold, metal complexation is a proven strategy to access new mechanisms of redox activity, biomolecule binding, and reactive oxygen species generation that can complement or enhance ligand-based pharmacology (Rijt and Sadler, 2009; Bruijnincx and Sadler, 2008; Allardyce et al., 2005; Rosenberg et al., 1965). In coordination chemistry, isatin can engage metal centers through oxygen and/or nitrogen donors, and representative binding patterns include monodentate, bidentate, and bridging motifs (Rodríguez-Argüelles et al., 1999; Raman et al., 2011). As a nitrogen-donor ligand, isatin undergoes a facile N–H bond activation, forming the isatinate ion. The frontier molecular orbitals (FMOs) of the isatinate ion (vide infra, Fig. 1) showed that it is a good σ-donor (HOMO-1 and HOMO-2), a π-donor (HOMO), and π-acceptor (LUMO+1, and LUMO+2). Additionally, the nitrogen and the adjacent carbonyl oxygen atoms are the most significant coordinating sites of the isatinate ion, as observed in Fig. 1, particularly when it acts as a bridging ligand.

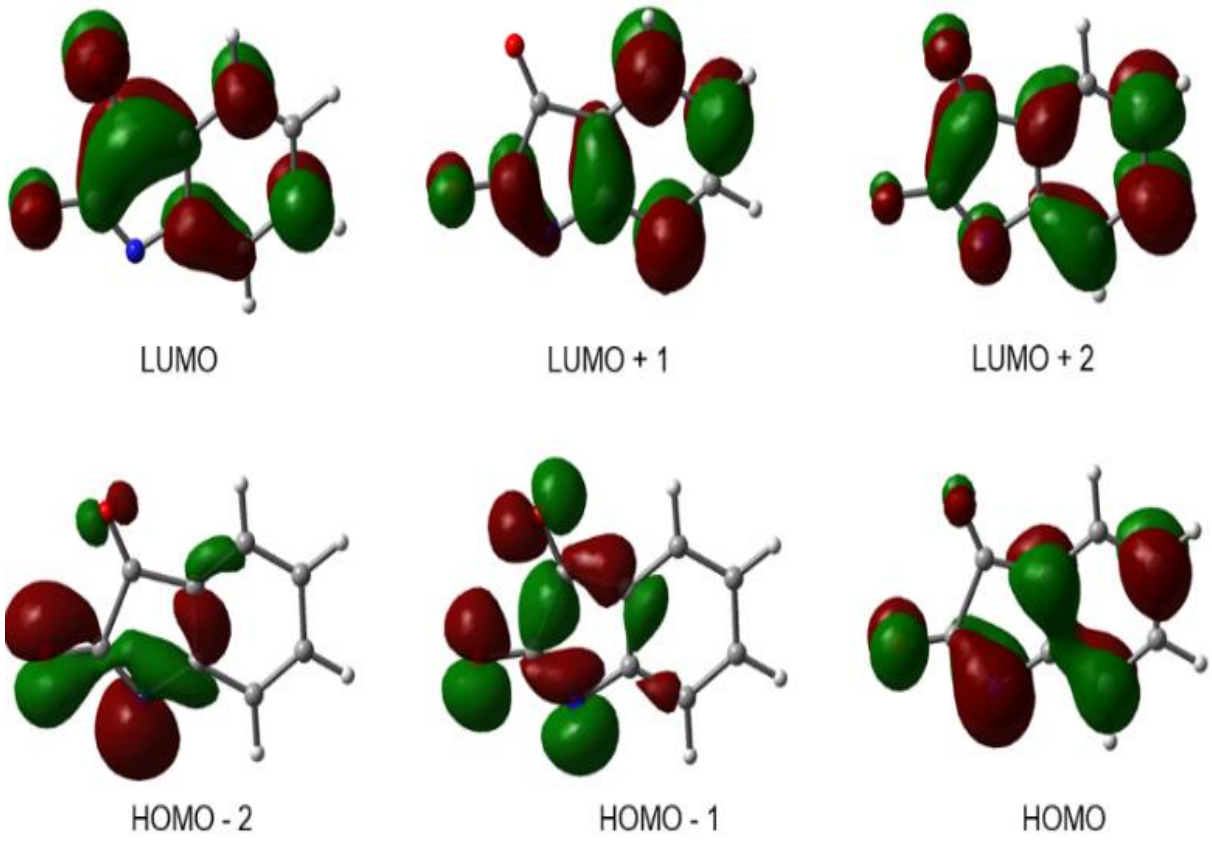

Fig. 1. FMOs of the isatinate ion generated by B3LYP/6-31G(d) level of theory.

Despite extensive work on isatin-derived chelators, structurally authenticated examples where the parent isatin binds in a bridging fashion to a metal–metal edge remain comparatively rare and therefore valuable (Hogarth and Norman, 1997). In this context, triosmium carbonyl clusters provide a particular interest because they can accommodate mixed donor ligation while maintaining a rigid triangular Os_3 core, allowing clear crystallographic identification of edge-spanning ligands and even the bridging hydrides (Darensbourg et al, 1989; Henderson et al., 1987; Lang et al., 1994; Eisenberg and Ibers, 1965). Based on this context, the reaction of $[Os_3(CO)_{10}(NCMe)_2]$ with isatin produces a hydrido-bridged triosmium isatinate cluster, in which the isatinate ion coordinates through the nitrogen and the adjacent carbonyl oxygen atom in a μ-(N,O) mode, as expected.

Experimental

General

The reactions were performed under a dry nitrogen atmosphere using standard Schlenk techniques. Solvents were dried and distilled over appropriate dehydrating agent and stored under nitrogen prior to use. Isatin was purchased from Aldrich Chemical Company and used without further purification. The labile precursor, $[Os_3(CO)_{10}(NCMe)_2]$, was prepared following published method (Nicholls and Vargas, 1989). Infrared spectra were measured in CH_2Cl_2 solution on a Shimadzu FTIR Prestige 21 spectrophotometer. ^{1}H NMR spectra were obtained in $CDCl_3$ using a Bruker Avance III HD (400 MHz) instrument and the chemical shifts were calculated with respect to residual solvent resonances. Elemental analyses for **1** were executed by standard microanalytical techniques. Compound **1** was isolated from the reaction mixture using preparative TLC coated with 0.25 mm of silica gel (HF254-type 60, E. Merck, Germany).

Synthesis of $[Os_3(CO)_{10}(\mu\text{-}H)(\mu\text{-}\kappa^1(O)\kappa^1(O)\text{-}C_6H_4(CO)_2N)]$ (1)

To a C_6H_6 solution (20 mL) of $[Os_3(CO)_{10}(MeCN)_2]$ (130.0 mg, 0.139 mmol) was added solid isatin (14.7 mg, 0.167 mmol), and the mixture was agitated under nitrogen atmosphere at ambient conditions for 18 h; during this time, the color changed to orange. The solvent was vaporized under low pressure and the residue was allowed to preparative thin-layer chromatography using silica. Eluting cyclo-C_6H_{12}:CH_2Cl_2 (2:3, v/v) developed one major band, which $[Os_3(CO)_{10}(\mu\text{-}H)(\mu\text{-}\kappa^1(O)\kappa^1(O)\text{-}C_6H_4(CO)_2N)]$ (1) (62.5 mg, 45%) as a deep yellow crystal from CH_2Cl_2/n-hexane mixture at –4 °C. Anal. Calcd. for $C_{18}H_5NO_{12}Os_3$: C, 21.66; H, 0.51 and N 1.40%, and experimentally found: C, 21.73; H, 0.57, N, 1.37%. IR (CH_2Cl_2, νCO, cm^{-1}): 2110 (w), 2069 (s), 2058 (w), 2019 (s), 1999(w), 1981(w). ^{1}H NMR ($CDCl_3$, ppm): 7.75 (d, J 6.0 Hz, 1H), 7.59 (t, J 6.0 Hz, 1H), 7.15 (t, J 6.0 Hz, 1H), 6.92 (d, J 6.0 Hz, 1H), −12.57 (s, 1H, μ-H).

X-ray crystallography

Single crystals of **1** suitable for x-ray diffraction analyses were obtained by slow diffusion of n-hexane into a CH_2Cl_2 solution of **1** at –4 °C. The crystal was mounted on a Bruker APEX3 microsource diffractometer with a nylon loop and paratone oil and data were collected at 210 K temperature with Mo-Kα radiation (λ = 0.71073). Data reduction and integration were performed using SAINT+ (Bruker, 2015), and absorption corrections were executed using SADABS (Bruker et al., 2014). The structure was solved with the ShelXS (Sheldrick, 2008) structure solution programs by direct and intrinsic phasing methods and refined by full-matrix least-squares based on F2 using SHELXL (Sheldrick, 2015) within the OLEX2 (Dolomanov et al., 2009) graphical user interface. All atoms other than hydrogens were refined anisotropically and the hydrogen atoms were added by the riding model. The hydride ligands were located from the difference Fourier map and refined isotropically. Experimental methods and notable structure parameters are summarized in Table 1.

Table 1. Crystal data, data collection methods, and structure refinement for $[Os_3(CO)_{10}(\mu\text{-}H)(\mu\text{-}\kappa^1(N)\kappa^1(O)\text{-}C_6H_4(CO)_2N)]$ (1).

Parameters	1
Empirical formula	$C_{18}H_5NO_{12}Os_3$
Formula weight	997.83
Temperature/K	210(2)
Crystal system	triclinic (Triclinic)
Space group	$P\ \bar{1}$
a/Å	7.791(6)
b/Å	7.987(5)
c/Å	18.347(11)
α/°	81.03(2)
β/°	89.30(3)
γ/°	71.808(17)
Volume/Å^3	1070.5(12)
Z	2
ρ_{calc} g/cm^3	3.096
μ/mm^{-1}	17.827
F(000)	888.0
Crystal size/mm^3	0.243 × 0.159 × 0.081
Radiation	Mo-Kα (λ = 0.71073)
2Θ range for data collection/°	4.5 to 54.28
Index ranges	$-9 \le h \le 9$ $-10 \le k \le 10$ $-23 \le l \le 23$
Reflections collected	27438
Independent reflections	4713 [R_{int} = 0.0345, R_{sigma} = 0.0234]
Data/restraints/parameters	4713/0/312
Goodness-of-fit on F^2	1.133
Final R indexes [I> = 2σ (I)]	R_1 = 0.0157, wR_2 = 0.0376
Final R indexes [all data]	R_1 = 0.0170, wR_2 = 0.0381
Largest diff. peak/hole / e Å^{-3}	0.822/–1.318

Computational study

The computational simulation was executed using the Gaussian 16 program (Frisch et al., 2019). Initial coordinates of **1** were generated from the CIF and optimized using gradient corrected density functional theory (DFT) method with a combination of Becke's three-parameter exchange functional (Becke, 1993) and Lee-Yang-Parr correlation functional (Lee et al., 1988). The osmium atoms were represented by Los Alamos National Laboratory (LANL) effective core potential (ECP) and a LanL2DZ basis set (Wadt and Hay, 1985), while a 6-31G(d) basis set was employed for the remaining elements (Rassolov et al., 2001). The dispersion correction was executed employing Grimme's D3 version of dispersion correction parameters in all calculations (Grimme et al., 2010). No imaginary frequency was found in the optimized geometry of the complex as expected, which corresponds to the true minima of its potential energy surfaces. The Wiberg bond indices (WBIs) of **1** were computed using natural bond orbital (NBO) analysis. The optimized geometry and the molecular orbitals were visualized using the Gauss view 6.0 program.

Results and discussion

Synthesis and spectroscopic characterization

Reaction of the labile triosmium precursor, $[Os_3(CO)_{10}(MeCN)_2]$, with isatin (1H-indole-2,3-dione) in benzene at room temperature resulted in efficient substitution of the labile acetonitrile ligands to give a hydrido bridged triosmium carbonyl isatinate compound $[Os_3(CO)_{10}(\mu\text{-}H)(\mu\text{-}\kappa^1(N)\kappa^1(O)\text{-}C_6H_4(CO)_2N)]$ (**1**) in 45% yield. The clean formation of this product under mild conditions indicates that isatinate ligand readily displaced coordinated MeCN and stabilized the $Os_3(CO)_{10}$ framework without inducing fragmentation or extensive carbonyl loss. Monitoring of the reaction by infrared spectroscopy shows the development of a new ν_{CO} pattern distinct from that of the starting material, consistent with

the formation of a substituted triosmium carbonyl cluster rather than a mixture of partially substituted intermediates.

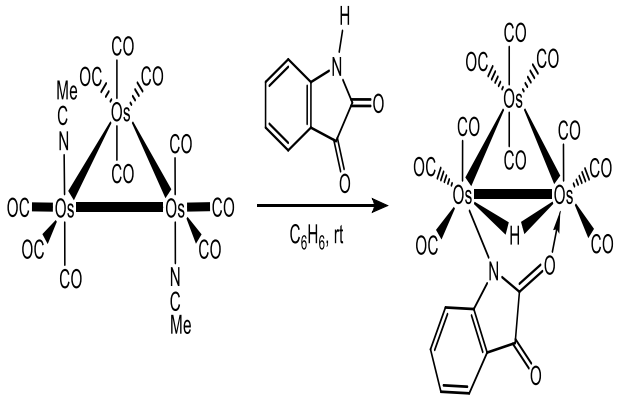

Scheme 2. Reaction of $[Os_3(CO)_{10}(MeCN)_2]$ with isatin.

The infrared spectrum displays six carbonyl stretching bands above 1850 cm^{-1}, consistent with the presence of terminal CO ligands and the absence of bridging carbonyls. The aromatic proton resonances in the ^1H NMR spectrum are found at 7.75 (d, J = 6.0 Hz, 1H), 7.59 (t, J = 6.0 Hz, 1H), 7.15 (t, J = 6.0 Hz, 1H), 6.92 (d, J = 6.0 Hz, 1H) for the isatinate moiety, and −12.57 (s, 1H) for the bridging hydride.

X-ray crystallography

The solid-state structure of **1** is depicted in Fig. 2, and selected bond distances and bond angles are mentioned in Table 2. The structure of **1** is defined by a isosceles triangle with two longer and almost equal Os–Os bond, which are even longer than the average Os–Os bond distance of 2.875(3) Å as observed in the parent $Os_3(CO)_{12}$ cluster (Corey and Dahl, 1962), while the rest one is shorter [Os(2)–Os(3) 2.8783 (14), Os(1)–Os(2) 2.928 (16), and Os(1)–Os(3) 2.9063 (14) Å]. An interesting feature of **1** is the coordination of the isatinate ligand to the cluster via the nitrogen atom and the adjacent carbonyl oxygen. Ten terminal CO groups are distributed in such a way that Os(3) has four, while each of the remaining Os atoms has three CO ligands. The vacant sites created by the removal of the MeCN ligands in the Os(1) and Os(2) atoms are compensated by the isatinate ligand, and the electron counts are balanced by the three electrons of the isatinate ligand and one from the bridging hydrogen atom. The structure of **1** displayed that the coordination behavior of the isatinate ligand is site-specific, i.e., only the nitrogen atom and the adjacent carbonyl oxygen atom coordinated to the metal atoms, keeping another oxygen atom free. However, this is expected because the FMOs of the isatinate ligand show more electron density on the nitrogen atom and the adjacent carbonyl oxygen atom (Fig. 1).

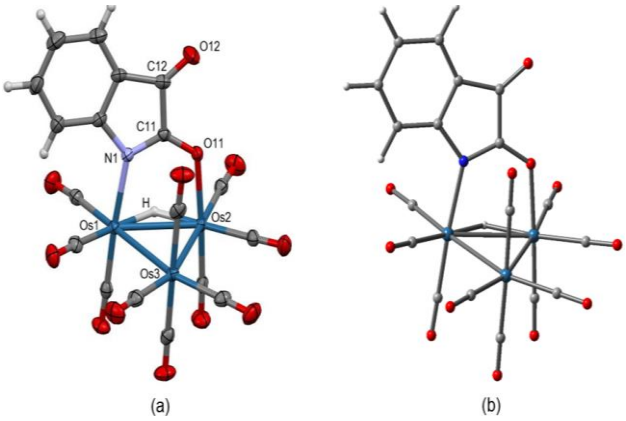

Fig. 2. The structure of 1. The ORTEP with the thermal ellipsoids 50% probability (a), and the DFT optimized geometry using B3LYP/6-31G(d)/LanL2DZ (for Os) level of theory (b).

Interestingly, the bridging hydride of **1** was crystallographically located and bridged the longest Os–Os vector. This is expected because the bonding between two metal atoms with a bridging hydride is a 3c-2e type as suggested by the computational study (vide infra). In **1**, the isatinate ligand bridged Os(2) and Os(3) from the axial coordination site, while the bridging hydride is almost coplanar with the Os_3 plane. All osmium cores of **1** adopt a slightly distorted octahedral geometry with six electron pairs about the central atoms.

Table 2. Notable bond distances (Å) and bond angles (°) of 1.

Bond/Angles	Value[a]	Value[b]
Os1–Os2	2.9128(16)	3.00028
Os1–Os3	2.9063(14)	2.98293
Os2–Os3	2.8783(14)	2.96344
Os1–N1	2.143(3)	2.17454
Os2–O11	2.129(2)	2.15773
N1–C11	1.314(4)	1.32912
C11–O11	1.259(4)	1.25832
Os3–Os1–Os2	59.29(2)	59.37723
Os3–Os2–Os1	60.24(3)	60.01991
Os2–Os3–Os1	60.47(4)	60.60286
N1–Os1–Os2	81.11(8)	80.23797
N1–Os1–Os3	91.69(8)	91.17388
O11–Os2–Os1	82.82(7)	81.86758
O11–Os2–Os3	91.18(7)	90.09329
O11–C11–N1	128.4(3)	128.23172
C11–N1–Os1	123.9(2)	124.57573
C11–O11–Os2	123.5(2)	124.63759

[a]Experimental, [b]Calculated from DFT optimized geometry

It is observed that the isatinate ligand originated in situ by the N–H bond activation, i.e., the isatin ligand was in the diketo form. This is supported by the observed Os(1)–N(1), Os(2)–O(11), C(11)–N(1), and C(11)–O(11) bond distances of 2.143(3), 2.129(2), 1.314(4) and 1.259(4) Å, respectively. However, the computational study on **1** shows a delocalization of the electron density over the nitrogen atom to the adjacent carbonyl oxygen atom (vide infra).

Computational study

The electronic structure and optimized geometry

The DFT-optimized geometry of **1** is displayed in Fig. 2b which is very close to its experimentally determined structure by X-ray crystallography. The DFT simulated bond lengths and angles are in good agreement with the experimental values. However, a few values are notably deviated. This is expected, as the actual structure is affected by experimental conditions such as temperature, pressure, solvent, and crystal packing whereas computational simulations are performed in a vacuum. The optimized geometry of the complex shows that the Os_3 core is in a distorted octahedral coordination sphere, while Os(3) and Os(3) are both in a distorted octahedral environment and weakly connected by Os⋯Os interaction. However, this is not a real 2c-2e Os–Os bond; rather, it is defined by the Os–H–Os bridged 3c-2e bond (vide infra). The latter case is supported by the longer Os⋯ Os separation observed in the structure of **1**.

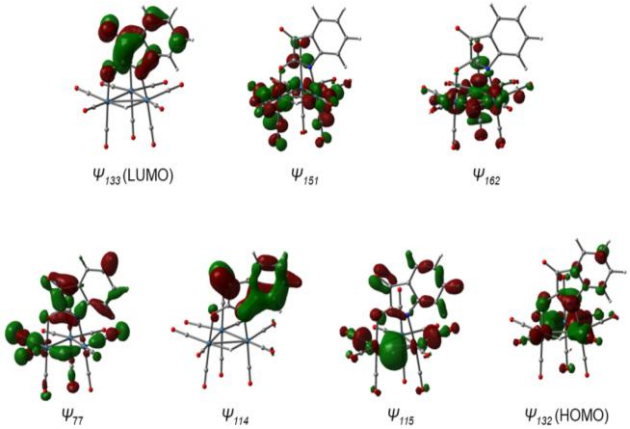

Fig. 3. Selected molecular orbitals of 1 generated by B3LYP/6-31G(d)/LanL2DZ (for Os) level of theory.

The crystal structure of **1** provides insight into the diketo tautomeric form of the istinate ligand: the nitrogen site forms a covalent Os–N bond, while the Os–O bond is a coordination bond. However, the molecular orbital (Ψ_{114} in Fig. 3) showed a delocalization of electron density. To explain the bond type, natural bond orbital (nbo) analysis was done. The calculated Wiberg bond indices (WBI) of N(1)–C(11) and C(11)–O(11) are 1.3645 and 1.3760, respectively, suggesting a delocalization of the π-electrons over the N(1) to O(11) atoms, e.g., partial double character of the N(1)–C(11) and C(11)-O(11) bonds. The WBI values for Os(1)–N(1) and Os(2)–O(11) are 0.5501 and 0.4817, respectively, all of which correspond to a single bond. The molecular

orbitals of **1** showed that the highest occupied molecular orbital (HOMO) is localized mainly on Os–Os and Os–C(O) bonds, whereas its lowest unoccupied molecular orbital (LUMO) spreads over the isatinate ligands (Fig. 3).

The three-centered two-electron (3c-2e) bonding. Structural investigation of clusters having a bridging hydride showed that the hydrido–bridged metal–metal edge is longer than the non-bridged metal–metal bond (Monira et al., 2015; Miah et al., 2026). A simple explanation of this phenomenon is in terms of the transfer of the metal–metal bonding electrons to the bridged hydrogen. However, a more precise explanation is the presence of a metal-H-metal 3c-2e bond. Based on a qualitative LCAO molecular orbital treatment for **1** presented here, we describe the Os-H-Os moiety as a three-center, two-electron (3c-2e) bridged bond. We account for all 48 valence electrons of **1** to describe the cluster bonding. As described earlier, each Os core is in a nearly octahedral coordination sphere. So, three atomic orbitals on each Os atom (d_{xy}, d_{yz} and d_{zx}) are considered to give nine nonbonding (or weakly bonding (π) and antibonding (π^*) by overlapping with the CO groups) molecular orbitals, which are all completely occupied. The remaining 18 valence atomic orbitals (6 on each Os atom) and 30 electrons are used to form Os–CO, Os–Os, Os–N, Os–O, and Os–H interactions. However, these interactions differ and are presented for conceptual purposes only, although they are in good agreement with the nearly octahedral geometry of each osmium core. Ten of these orbitals are used for Os–CO σ-bonding. Two of the remaining orbitals are used to form Os(2)–N and Os(3)–O σ-bonding. Linear combinations of the remaining two atomic orbitals on Os(3) and one atomic orbital from each of Os(1) and Os(2), form two bonding and two antibonding molecular orbitals. Filling the two bonding molecular orbitals gives formal bond orders of **1** for the two shorter edges of the triosmium framework. The two remaining atomic orbitals (particularly the d_z2 orbital) on Os(2) and Os(3) are oriented toward the bridging hydrogen atom. A linear combination of these two orbitals gives one bonding and one antibonding combination. Linear combination of the bonding combination of the Os_2 fragment and the s atomic orbital of the bridging hydride gives a bonding and an antibonding molecular orbital for the Os–H–Os fragment of **1**. The antibonding combination of the Os_2 fragment remains non-bonding in the formation of Os–H–Os, as its symmetry does not match the hydrogen *s* atomic orbitals. A quantitative molecular orbital diagram for the formation of the Os–H–Os fragment of **1** by the linear combination of the Os_2 fragment and the *s* atomic orbital of the bridging hydrogen atom is depicted in Fig. 4.

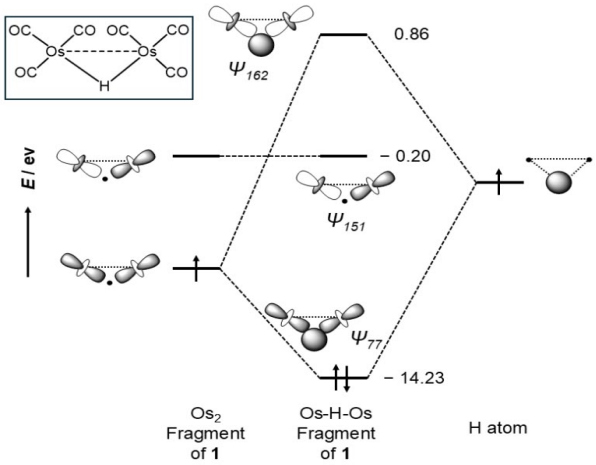

Fig. 4. A quantitative MO diagram for the Os–H–Os fragment bonding in 1. The energies of the MOs are calculated by B3LYP/6-31G(d)/Lan-L2DZ (for Os) level of theory.

If we consider that the nitrogen atom of the isatinate ligand is a single electron donor, the Os_2 fragment would hold a single electron in its lower energy bonding-type fragment orbital. This would result in a single electron on the bridging hydrogen atom. Their combination results in a pair of electrons which occupies the lower energy bonding type combination of the Os–H–Os fragment of **1** (Fig. 4). This would result in the spread of an electron pair among Os(2), H, and Os(3) atoms, i.e., the three centered two electron (3c-2e) bonding in 1 (Fig. 3). The calculated WBI values of Os(1)–Os(2), Os(1)–H and Os(2)-H are 0.4590, 0.5192 and 0.5059 respectively, which is consistent with the 3c-2e bonding in Os(1)–H–Os(2) fragment of **1**. The crystal structure of **1** showed one

equatorial CO group on each of the Os(1) and Os(2) atoms opposite to the bridging hydride; no CO groups opposite to the Os(1)–Os(2) vector. This suggested that the more electrons on Os(1)–H and Os(2)–H bond with a negligible electron density for direct Os(1)–Os(2) bond.

Conclusion

A noble hydrido-bridged triosmium isatinate complex, $[Os_3(CO)_{10}(\mu\text{-}H)(\mu\text{-}\kappa^1(N)\kappa^1(O)\text{-}C_6H_4(CO)_2N)]$ (**1**) was formed from the room temperature reaction of $[Os_3(CO)_{10}(MeCN)_2]$ with isatin. The structure of **1** was ascertained by spectroscopy, crystallography, and DFT calculations. The electronic structure of **1** was determined computationally, revealing a three-centred-two-electron (3c-2e) Os–H–Os bond. The aesthetic coordination mode of the isatinate ligand gives insight into the future design and development of noble complexes with Os–N, Os–O, and Os–H–Os 3c-2e bridged bonds.

Acknowledgment

The financial support from the Ministry of Science and Technology, Bangladesh, is gratefully acknowledged. We thank Dr. Vladimir N. Nesterov, University of North Texas, for solving the X-ray structure, and Mr. Nikhil Bhoumik, Wazed Miah Science Research Center, for X-ray intensity data collection. SI is thankful to Professor K.-i. Sugiura, Tokyo Metropolitan University, Japan, for his support of computational chemistry.

Authors contribution

MMA:Investigation, Writing original draft; SI: Computational study, Writing and editing; NA: Investigation, Writing original draft; SEK: Conceptualization, Supervision and Editing.

Conflict of interest

The authors declare no competing interests.

Supplementary information

CCDC 2532447 refers to the crystallographic data for the title complex, 1. Copy of this data can be obtained free of charge via https://www.ccdc.cam.ac.uk/-conts/retrieving.html (or from Cambridge Crystallographic Data Centre, 12 Union Road, Cambridge CB2 1EZ, UK (Tel: +441223 336408; fax: +44 1223 336033; email: deposit@ccdc.cam.ac.uk)).

References

Allardyce CS, Dorcier A, Scolaro C, and Dyson PJ. Development of organometallic (organo-transition metal) pharmaceuticals. *Appl. Organomet. Chem*. 2005; 19: 1–10.

Becke AD. Density-functional thermochemistry. III. The role of exact exchange. *J. Chem. Phys.* 1993; 98: 5648–5652.

Bruijnincx PCA and Sadler PJ. New trends in medicinal inorganic chemistry. *Curr. Opin. Chem. Biol*. 2008; 12: 197–206.

Bruker SADABS-2014/5, Bruker AXS Inc. 2014, Madison, Wisconsin, USA.

Bruker SAINT (8.37A), Bruker AXS Inc. 2015, Madison, Wisconsin, USA.

Corey ER. and Dahl LF. The Molecular and Crystal Structure of $Os_3(CO)_{12}$. *Inorg. Chem.* 1962; 1: 521–526.

Darensbourg MY, Liaw W, and Riordan CG. Metal–sulfur bonding in transition-metal complexes. *J. Am. Chem. Soc*. 1989; 111: 8051–8052.

Dolomanov OV, Bourhis LJ, Gildea RJ, Howard JAK, and Puschmann H. OLEX2: A Complete Structure Solution, Refinement and Analysis Program. *J. Appl. Crystallogr.* 2009; 42: 339–341.

Eisenberg R and Ibers JA. Metal–metal interactions in carbonyl complexes. *J. Am. Chem. Soc*. 1965; 87: 3776–3781.

Frisch MJ, Trucks GW, Schlegel HB, Scuseria GE, Robb MA, Cheeseman JR, Scalmani G, Barone V, Petersson GA, Nakatsuji H, Li X, Caricato M, Marenich AV, Bloino J, Janesko BG, Gomperts R, Mennucci B, Hratchian HP, Ortiz JV, Izmaylov AF, Sonnenberg JL, Williams-Young D, Ding F, Lipparini F, Egidi F, Goings J, Peng B, Petrone A, Henderson T, Ranasinghe D, Zakrzewski VG, Gao J, Rega N, Zheng G, Liang

W, Hada M, Ehara M, Toyota K, Fukuda R, Hasegawa J, Ishida M, Nakajima T, Honda Y, Kitao O, Nakai H, Vreven T, Throssell K, Montgomery JA Jr, Peralta JE, Ogliaro F, Bearpark MJ, Heyd JJ, Brothers EN, Kudin KN, Staroverov VN, Keith TA, Kobayashi R, Normand J, Raghavachari K, Rendell AP, Burant JC, Iyengar SS, Tomasi J, Cossi M, Millam JM, Klene M, Adamo C, Cammi R, Ochterski JW, Martin RL, Morokuma K, Farkas O, Foresman JB, and Fox DJ. Gaussian 16, Revision C.01, Gaussian, Inc., 2019, Wallingford CT.

Grimme AS, Antony J, Ehrlich S, and H. Krieg (2010). Consistent and accurate *ab initio* parametrization of density functional dispersion correction (DFT-D) for the 94 elements H-Pu. *J. Chem. Phys.* 2010; 132: 154104.

Henderson RA, Hughes DL, Richards RL, and Shortman C. Sulfur-donor ligands in transition-metal carbonyl clusters. *J. Chem. Soc., Dalton Trans*. 1987; 1115–1122.

Hoff CD. Reactivity of metal–sulfur complexes. *Prog. Inorg. Chem.* 1992; 40: 503–561.

Hogarth G and Norman T. Metal carbonyl cluster reactivity. *Inorg. Chim. Acta*. 1997; 254: 167–175.

Ju TD, Capps KB, Roper GC, Lang RF, and Hoff CD. Reactivity of metal carbonyl clusters with heterocyclic ligands. *Inorg. Chim. Acta*. 1998; 270: 488–495.

Lang RF, Ju TD, Kiss G, Hoff CD, Bryan JC, and Kubas GJ. Carbonyl cluster chemistry of transition metals. *Inorg. Chem*. 1994; 33: 7917–7924.

Lee C, Yang W, and Parr RG. Development of the Colle-Salvetti correlation-energy formula into a functional of the electron density. *Phys. Rev. B*, Condens. Matter. 1988; 37(2): 785–789.

Medvedev A, Buneeva O, and Glover V. Biological effects of isatin. *Biol*. 2007; 1: 151-162.

Miah MJA, Rahaman MM, Islam MW, Siddiquee TA, Islam S, and Karim MM. Facile C–H bond activation of 2-ethylmercaptobenzothiazole in a tri-smium carbonyl cluster: Crystal structure of $Os_3(CO)_{10}(\mu\text{-}H)\{\mu_{N,C}\text{-}NC(SC_2H_5)SC_6H_3\}$. *J. Chem. Crystallogr*. 2026; 56: 5.

Monira S, Afrin S, Azam KA, Hossain MK, Tocher DA, Ghosh S, Rajbangshi S, Kabir SE, and Hogarth G. Oxidative-addition of the N–H bond of saccharin (sacH) to a triosmium centre: Synthesis, structure and reactivity of $Os_3(CO)_{10}(\mu\text{-}H)(\mu\text{-}sac)$. *J. Organomet. Chem*. 2015; 799–800: 281–290.

Nicholls JN and Vargas MD. Some useful derivatives of dodecacarbonyltriosmium. *Inorg. Synth*. 1989; 26:289–293.

Raman N, Pothiraj K, and Baskaran T. Metal complexes derived from bioactive ligands. *J. Coord. Chem.* 2011; 64: 3900–3912.

Rassolov VA, Ratner MA, Pople JA, Redfern PC, and Curtiss LA. 6-31G* basis set for third-row atoms. *J. Comput. Chem*. 2001; 22: 976–984.

Rijt SHv and Sadler PJ. Current applications of metal complexes in drug discovery. *Drug Discov. Today*. 2009; 14: 1089–1097.

Rodríguez-Argüelles MC, Sánchez A, Ferrari MB, Fava GG, Pelizzi C, Pelosi G, Albertini R, Lunghi P, and Pinelli S. Transition-metal complexes of isatin-β-thiosemicarbazone. X-ray crystal structure of two nickel complexes. *J. Inorg. Biochem.* 1999; 73: 7–15.

Rosenberg B, VanCamp L, and Krigas T. Inhibition of cell division by platinum compounds. *Nat*. 1965; 205: 698–699.

Russell FL, Ju D, Elvin T, Jeffrey CB, Gregory JK, and Hoff CD. Reactivity of heterocyclic ligands with metal carbonyls. *Inorg. Chim. Acta*. 2003; 348: 157–165.

Sheldrick GM. A Short History of SHELX. *Acta Crystallogr*. 2008; 64: 112–122.

Sheldrick GM. Crystal Structure Refinement with SHELXL. *Acta Crystallogr*. 2015; 71: 3–8.

Silva JFMd, Garden SJ, and Pinto AC. Chemistry of isatin derivatives. *J. Braz. Chem. Soc*. 2001; 12: 273–280.

Stiefel EI and Matsumoto K. Transition metal sulfur chemistry. *ACS Symposium Ser*. 1996; 653: 1–25.

Vine KL, Matesic L, Locke JM, Ranson M, and Skropeta D. Cytotoxic and anticancer activities of isatin and its derivatives: a comprehensive review from 2000-2008. *Anticaner Agents Med. Chem.* 2009; 9: 397–414.

Wadt WR and Hay PJ. *Ab initio* effective core potentials for molecular calculations. Potentials for the transition metal atoms Sc to Hg. *J. Chem. Phys.* 1985; 82: 270–283.

Wadt WR and Hay PJ. *Ab initio* effective core potentials for molecular calculations. Potentials for K to Au, including the outermost core orbitals. *J. Chem. Phys.* 1985; 82: 299–310.

Wadt WR and Hay PJ. *Ab initio* effective core potentials for molecular calculations. Potentials for main group elements Na to Bi. *J. Chem. Phys.* 1985; 82: 284–298.